Biosensors and Bioelectronics 130 (2019) 254–261

Contents lists available at ScienceDirect

Biosensors and Bioelectronics

journal homepage: www.elsevier.com/locate/bios

MnO_2 nanosheets as the biomimetic oxidase for rapid and sensitive oxalate detection combining with bionic E-eye

Ying Gan[a,b,1], Ning Hu[a,1], Chuanjiang He[a], Shuqi Zhou[a], Jiawei Tu[a], Tao Liang[a], Yuxiang Pan[a], Dmitry Kirsanov[c], Andrey Legin[c], Hao Wan[a,b,*], Ping Wang[a,b,*]

[a] Biosensor National Special Laboratory, Key Laboratory of Biomedical Engineering of Ministry of Education, Department of Biomedical Engineering, Zhejiang University, Hangzhou 310027, China
[b] State Key Laboratory of Transducer Technology, Chinese Academy of Sciences, Shanghai 200050, China
[c] Laboratory of Chemical Sensors, Chemistry Department, Mendeleev Center, Saint-Petersburg State University, Saint-Petersburg 199034, Russia

ARTICLE INFO

Keywords:
Oxalate
3,3',5,5'-tetramethylbenzidine
MnO_2 nanosheets
Bionic E-eye
Colorimetric detection

ABSTRACT

Urolithiasis commonly occurs in kidney and ureteral, and may cause local organ/tissue damage, even kidney failure. The incidence of this disease is increasing worldwide, in which calcium oxalate is the major composition forming the urinary calculus. Therefore, to monitor this disease for the prevention and treatment, measuring the oxalate in the urine is of great significance. Here, a rapid and sensitive colorimetric method was developed based on 3,3',5,5'-tetramethylbenzidine-manganese dioxide (TMB-MnO_2) nanosheets for oxalate detection. MnO_2 nanosheets acted as an efficient biomimetic oxidase to catalyze the reaction with TMB and oxalate. Pale yellow TMB can be oxidized to blue oxide TMB catalyzed by BSA-stabilized MnO_2 nanosheets, and oxalate can selectively inhibit this reaction by consuming and reacting with MnO_2 nanosheets, thus achieving the quantitative detection of oxalate. Moreover, a home-made bionic electronic-eye (E-eye) system was developed as a portable in-situ detection platform to efficiently measure the oxalate concentrations in 10 s by direct photographing. By optimizing experimental conditions, this method shows a wide linear range (7.8 μM to 250 μM) and a low detection limit (0.91 μM) for oxalate detection. Besides, this method exhibits high selectivity even with 80-fold interfering chemicals. Furthermore, the performance of the method was validated by testing the artificial urine samples, indicating its great potential for monitoring and diagnosis of urolithiasis in point-of-care applications.

1. Introduction

Urolithiasis is a common disease of the urinary system that can cause urinary tract obstruction, local organ damage and even kidney failure, during which calculus can be observed in any part of the kidney, bladder, ureter and urethra. Due to the extreme heat and water shortages worldwide, the incidence of urolithiasis is increasing all over the world (Romero et al., 2010; Turney et al., 2012). In developed countries, the lifetime prevalence of urolithiasis is about 10%, and mainly occur in the middle of adulthood (Akoudad et al., 2010; Boyce et al., 2010; Stamatelou et al., 2003). The probability of stone formations around the world varies from 1% to 5% in Asia, 5–9% in Europe, and 13% in North America (Mitra et al., 2018). Meanwhile, ureteral stones account for 5–10% of the total population, and the prevalence rate is still on the rise (Somani et al., 2016). The calculus diseases is formed due to the deposition of crystals in the kidney, which mainly consist calcium oxalate, calcium phosphate, calcium carbonate, magnesium ammonium phosphate, uric acid and cysteine (Parmar, 2004). It is worth stressing crystals in that 85% urolithiasis mainly contain calcium oxalate (Coe et al., 2016). Normal oxalate levels in healthy people is 100–300 μM in urine (Pundir and Satyapal, 1998) and 0.8–2.50 μM in plasma (Pundir et al., 1998). The excess concentration of oxalate in urine (> 300 μM) indicates the high suspicion of urolithiasis. Therefore, an accurate, efficient, and rapid method for measuring oxalate is of great necessity to prevent and diagnose urolithiasis in the early stage.

A variety of methods have been developed to measure oxalates in food, urine or plasma, such as spectrophotometry (Zhai et al., 2006; Zuo et al., 2010), ion chromatography (Maya et al., 2011), amperometric biosensor (Pundir et al., 2011), capillary electrophoresis (Munoz et al., 2010), high-performance liquid chromatography (Perello et al., 2005),

* Corresponding authors at: Biosensor National Special Laboratory, Key Laboratory of Biomedical Engineering of Ministry of Education, Department of Biomedical Engineering, Zhejiang University, Hangzhou 310027, China.
E-mail addresses: wh1816@zju.edu.cn (H. Wan), cnpwang@zju.edu.cn (P. Wang).
[1] These authors contribute equally to this work.

https://doi.org/10.1016/j.bios.2019.01.026
Received 26 September 2018; Received in revised form 9 December 2018; Accepted 7 January 2019
Available online 21 January 2019
0956-5663/

and gas chromatography (Li et al., 2008). However, most of the above analytical techniques for determining oxalate depend on expensive and complex equipment, large numbers of samples, toxic and expensive reagents, or an expert technician. Moreover, it is significant to develop a method that can be applied to measure urinary oxalate for point-of-care applications. Thus, some colorimetric and fluorescent sensors have been developed for rapid oxalate detection. (Dey et al., 2018; Inoue et al., 2018; Worramongkona et al., 2018; Zhang et al., 2014). However, spectrophotometers with large size and time-consuming measurement hamper the point-of-care applications.

Recently, some studies reported that MnO_2 nanomaterials possessed intrinsic oxidase-like activity (Liu et al., 2012; Wan et al., 2012). Because 3,3',5,5'-tetramethylbenzidine (TMB) can be oxidized from a pale yellow to a blue oxide TMB, it can be used as an indicator of the reaction with MnO_2 nanomaterials. Also, TMB, as a specific detection agent, was proposed to detect MnO_2 nanosheets (He et al., 2016), which provides more possibilities for the application of the TMB- MnO_2 nanosheets system. The system has been used in many quantitative measurements such as H_2O_2 and glucose in blood (Yuan et al., 2015), ascorbic acid (Yu and Zheng, 2016) single-stranded DNA (Lin et al., 2016), and glutathione (GSH) in human serum (Liu et al., 2017).

Herein, a rapid and sensitive colorimetric method based on TMB-MnO_2 nanosheets for oxalate detection was developed combining with a highly portable bionic E-eye system (Fig. 1). MnO_2 nanosheets acted as an efficient biomimetic oxidase to catalyze the reaction with TMB and oxalate. First, the prepared bulk MnO_2 was exfoliated in a BSA solution by sonication to obtain the MnO_2 nanosheets. The BSA-stabilized-MnO_2 nanosheets feature good dispersion and stability. The nanosheets can be used to oxidize TMB to oxTMB, resulting in the color change of the substrate from pale yellow to blue. In the presence of oxalate, MnO_2 nanosheets were reduced by oxalate, and the amount of residual nanosheets used to oxidize TMB decreased, thus leading to different color changes that can be quantified for oxalate measurements. Moreover, a home-made colorimetric system called bionic E-eye was utilized to identify the color changes by direct photographing, and analyze the concentration of oxalate, which realizes the function of rapid detection and portability. Furthermore, to verify the feasibility of the method for real sample analysis, the selectivity of the method and the performance for real sample measurement were both studied.

2. Experimental and methods

2.1. Chemicals and reagents

All reagents used in this work were analytical grade unless otherwise noted. Manganese (II) chloride tetrahydrate ($MnCl_2{\cdot}4H_2O$), 3,3',5,5'-tetramethylbenzidine (TMB), tetramethylammonium hydroxide solution(25% TMA·OH), 30% H_2O_2, bovine serum albumin (BSA), urea, creatinine, sodium oxalate were purchased from Aladdin Reagent Co., Ltd (China). NaCl, KCl, glucose, $Na_2HPO_4{\cdot}12H_2O$, $NaH_2PO_4{\cdot}2H_2O$, NH_4Cl, $MgSO_4$ and sodium citrate were purchased from Sinopharm Chemical Reagent Co., Ltd (China). The kit for oxalate detection was purchased from Shanghai Enzyme-linked Biotechnology Co., Ltd. Ultrapure water was produced by a Millipore Milli-Q water purification system.

2.2. Apparatus

Ultraviolet-visible light (UV–vis) absorption spectra were recorded by Nanodrop 2000 (Thermo Scientific, USA). The morphology of bulk MnO_2 was determined using Desktop scanning electron microscopy (DSEM, Phenom PROX, Netherlands). MnO_2 nanosheets were characterized using a JEM-2100 transmission electron microscope (TEM, JEOL, Japan) with an accelerating voltage of 200 kV. Mn^{2+} ion was characterized by ion chromatograph (AQUION IC, Thermo Scientific) and pH meter (INESA Scientific Instrument Co.,Ltd, China) was used for pH measurement in samples. The detection of oxalate was performed with the SpectraMax Paradigm multi-mode microplate reader (MR, Molecule Device, USA) and the home-made bionic E-eye developed in our laboratory.

The bionic E-eye was consisted of a smartphone and a portable illumination provider. The illuminated area on the electroluminescent

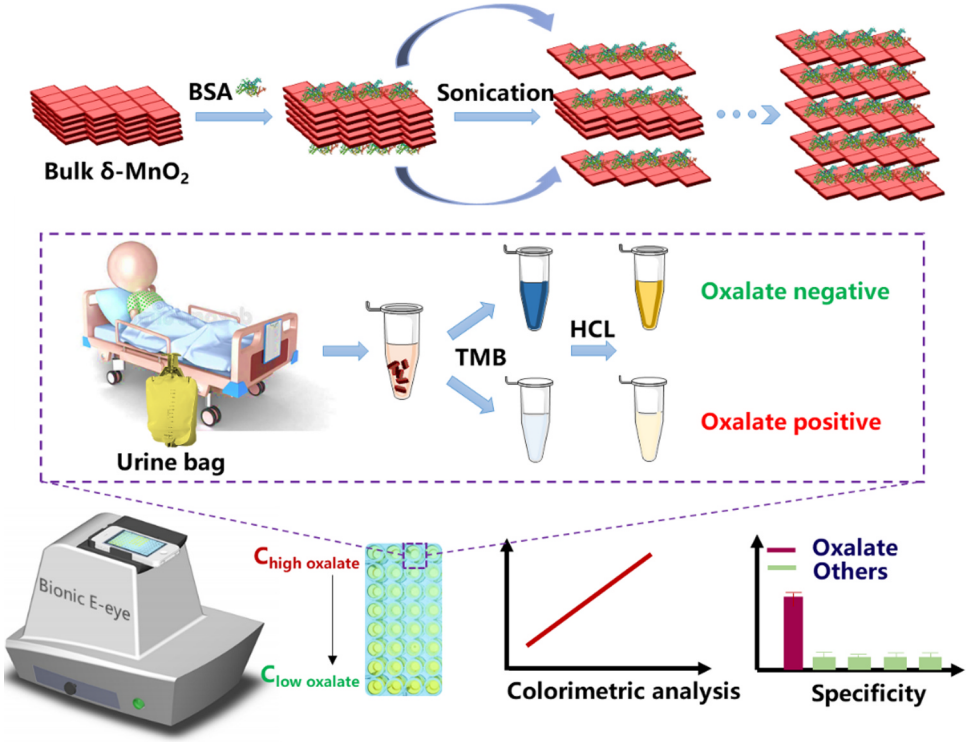

Fig. 1. Schematic of TMB-MnO_2 nanosheets for colorimetric oxalate detection by bionic E-eye system.

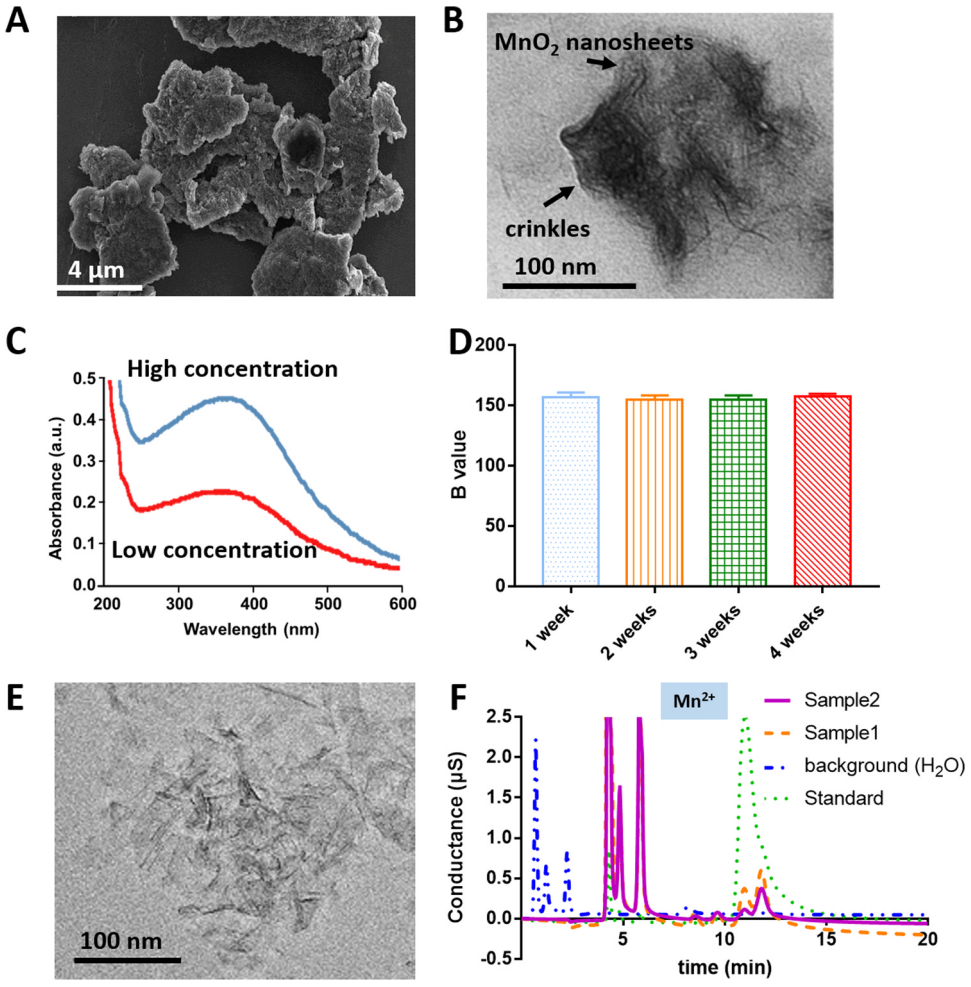

Fig. 2. (A) SEM image of the bulk MnO_2 material. (B) TEM image of the original MnO_2 nanosheets. (C) UV–vis spectrum of two MnO_2 nanosheets solutions (the concentration of one solution (blue) is 2-fold of the other one (red)). (D) The stability of MnO_2 nanosheets. (E) TEM of MnO_2 nanosheets after oxalate incubation (F) Characterization of the formation of Mn^{2+} by ion chromatograph. (For interpretation of the references to color in this figure legend, the reader is referred to the web version of this article).

source was designed to place 96-well plates that contained colorimetric end-products. The smartphone, utilized as the measurement instrument, can photograph the plates by placing inside a designated smartphone container on the top of the hood. Finally, a square image (10 × 10 pixels) of each well was extracted from the captured image, and the RGB value can be calculated for colorimetric analysis (Su et al., 2015). Before the image analysis, the blank plate will be photographed for baseline calibration. In this work, the blue value (B value) was used to analyze color change.

2.3. Synthesis of bulk MnO_2 and MnO_2 nanosheets

The preparation of bulk MnO_2 was performed according to the literature (Kai et al., 2008). 10 ml 0.3 M $MnCl_2{\cdot}4H_2O$ aqueous solution was added into 20 ml mixture (0.6 M TMA·OH and 3 wt% H_2O_2), and the resulting solution was dark brown. The solution was stirred vigorously on a shaker at 25 °C. After stirring for 12 h, the solution was centrifuged at 10000 rpm for 10 min. The precipitate was extracted out and washed with methanol and ultrapure water for three times. Subsequently, the precipitate was dried in a vacuum oven at 30 °C.

Some researchers prepared MoS_2 nanosheets by exfoliating MoS_2 powders with BSA (Guan et al., 2015). By utilizing the similar mechanism, the MnO_2 nanosheets were obtained by exfoliating bulk MnO_2 with BSA. The bulk MnO_2 is formed due to the van der Waals force between layers. By sonication, the van der Waals force was weakened, and layers were ultimately peeled off to form nanosheets (Liu et al., 2007). The reason is that high temperature and pressure are generated inside the collapsing microbubbles during the sonication, which promotes the intercalation of BSA into the layered MnO_2. Nanosheet synthesis steps are as follows. 10 mg bulk MnO_2 was added to 10 ml 1 mg/ml BSA aqueous solution. After that, the mixture was sonicated for 8 h at room temperature. Then, the solution was centrifuged at 1000 rpm for 20 min. The precipitate containing residual unexfoliated MnO_2 was removed, and the supernate containing MnO_2 nanosheets was obtained and stored at 4 °C.

2.4. Oxalate detection and image analysis by bionic E-eye

Sodium oxalate solution (40 mM) was prepared and adjusted to pH = 3 using H_2SO_4 (pH = 1.0). 3 μl MnO_2 nanosheets were incubated in 100 μl oxalate solution for 10 min to ensure complete reaction. Then, 100 μl TMB solution was added into the above mixture to implement

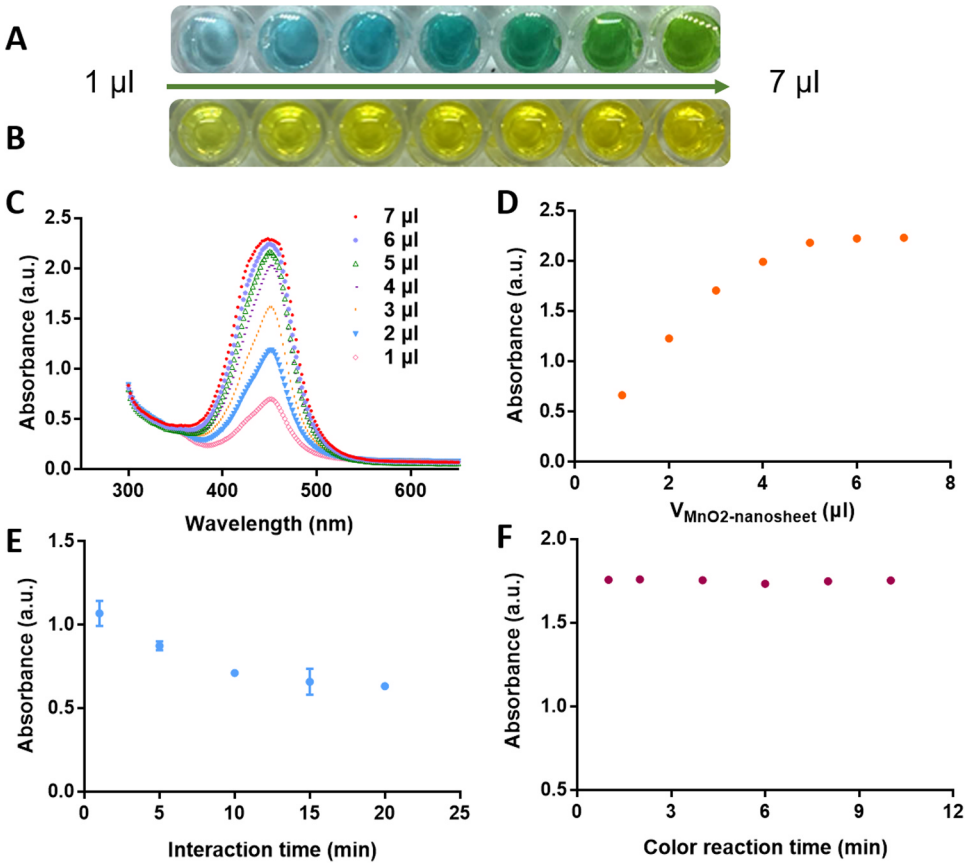

Fig. 3. Color changes of the TMB solution incubated with MnO_2 nanosheets in the (A) absence and (B) presence of HCl. (C) Absorbance spectra of TMB incubated with different volume of MnO_2 nanosheets after HCl was added. (D) The plot of the peak absorbance with different volume of MnO_2 nanosheets. (E) Effect of the interaction time between oxalate and MnO_2 nanosheets on the detection of 100 μM oxalate. (F) The absorbance change with different color reaction time after TMB was added into the MnO_2 nanosheets solution. All experiments were repeated in 5 well with error bars in (D), (E), (F). (For interpretation of the references to color in this figure legend, the reader is referred to the web version of this article).

reactions for 1 min. After the reaction, 100 μl 1 M HCl was added into the solution to stop the reaction process. All reactions were performed in 96-well plates. Finally, the plate was placed into the bionic E-eye for colorimetric analysis. Through image processing and color analysis, the concentration of oxalate can be determined.

2.5. Detection of oxalate in artificial urine samples

Oxalate concentration in artificial urine samples was quantified by the method to evaluate the practical applications of the biosensor. The artificial urine sample without oxalate was prepared according to the literature (Chutipongtanate and Thongboonkerd, 2010), which contains 0.45 g creatinine, 2.25 g KCl, 0.50 g $MgSO_4{\cdot}7H_2O$, 1.48 g $Na_3C_6H_5{\cdot}7H_2O$, 3.17 g NaCl, 0.17 g $NaHCO_3$, 0.05 g $Na_2HPO_4{\cdot}12H_2O$, 0.05 g $NaH_2PO_4{\cdot}2H_2O$, 1.29 g of Na_2SO_4, 0.80 g of NH_4Cl, 12.13 g urea and 0.17 g uric acid in 1000 ml deionized water. Then the artificial urine sample was diluted 30 times and adjusted to pH = 3. 40 mM oxalate solution was diluted using the diluted artificial urine sample to different concentration (25 μM, 50 μM, 100 μM). The analysis of each sample was repeated for 3 times. Moreover, the kit was used also for comparison. The kit uses a double antibody sandwich method to determine the level of oxalate in the sample. TMB is converted to blue under the catalysis of HRP-labeled antibody and converted to the final yellow color by the action of an acid. The depth of the color is positively correlated with the concentration of oxalate in the sample. The absorbance was measured at 450 nm using a plate reader, and the oxalate content in the sample was calculated based on the standard curve.

3. Results and discussion

3.1. Characterization of MnO_2 nanosheets and MnO_2-oxalate colorimetric assay

As reported in the presence of TMA·OH, bulk MnO_2 was synthesized by the oxidization of Mn^{2+} with H_2O_2 (Kai et al., 2008). Fig. 2 (A) presents the SEM image of the bulk MnO_2, in which typical bulk structure can be observed.

For MnO_2 nanosheet exfoliation, the amount of BSA is extremely critical. Guan et al. has reported that low concentration of BSA in form of monomers can strongly adsorb on bulk MoS_2, leading to the effective exfoliation MoS_2 nanosheets by sonication (Guan et al., 2015) However, BSA with high concentration (> 4 mg/ml) aggregate and cannot strongly adsorb on bulk MoS_2, leading to the ineffective exfoliation of MoS_2 nanosheets. It is reported that 1 mg/ml BSA was used to exfoliated 10 mg MnO_2 effectively (Liu et al., 2017). Thus, the same BSA amount was used in this study to exfoliate MnO_2. Fig. 2(B) shows the TEM image of exfoliated MnO_2 nanosheets in which a large planar and ultrathin sheet with occasional crinkles can be observed. Two MnO_2 nanosheets solutions were measured with the UV–vis absorption spectrum in the range of 200–600 nm as shown in Fig. 2(C), in which the concentration of one solution (blue) is 2-fold of the other one (red). According to the UV–vis absorption spectrum, the absorption peak of MnO_2 nanosheets can be observed at 380 nm, which indicates the characteristic peak of MnO_2 nanosheets. This characteristic peak of the prepared MnO_2 nanosheets agrees with the previous work (Zhai et al., 2014), which validates the expected exfoliation of MnO_2 nanosheets in

this work. The concentration of the stock MnO_2 nanosheets was calculated based on the UV–vis results according to the Beer-Lambert Law (Eq. (1)):

$$A = \lg\left(\frac{1}{T}\right) = Kbc, \quad (1)$$

where A is the absorbance, T is the transmittance, K is the molar extinction coefficient (for MnO_2 nanosheets, $K = 9.6 \times 10^3\ M^{-1}\ cm^{-1}$ at 380 nm), b is the sample thickness and c is the sample concentration. The concentration of the prepared MnO_2 nanosheets is calculated as 1.84 mM. Moreover, the prepared MnO_2 nanosheets solution displayed apparent dark brown color. Furthermore, to verify the stability of MnO_2 nanosheets, the oxidization of MnO_2 nanosheets was also investigated over 4 weeks, and no significant change in the absorbance was observed shown in Fig. 2 (D), suggesting that the oxidation capability of the MnO_2 nanosheets to TMB remains constant, and the MnO_2 nanosheets can be stored for a long term with good chemical stability.

Oxalate has been shown to reduce MnO_2 and form Mn^{2+} (Xyla et al., 1992) (Eq. (2)):

$$MnO_2 + C_2O_4^{-2} + 4H^+ \rightarrow Mn^{2+} + 2CO_2 + 2H_2O \quad (2)$$

Therefore, when MnO_2 nanosheets were added to the oxalate, MnO_2 nanosheets were consumed and reduced to Mn^{2+}, which affects the colorimetric reaction with TMB. To further validate the reaction, MnO_2 nanosheets were examined by TEM shown in Fig. 3(E). Compared with the MnO_2 nanosheets before the reaction (Fig. 3(C)), the outline of the nanosheets becomes blurred and thickness becomes thin with a low contrast in TEM image after oxalate incubation. The samples after the reaction were also analyzed by ion chromatograph to validate the formation of Mn^{2+} (Fig. 3(F)). The four curves in the figure are the test results of the standard sample ($MnCl_2$, 5 mM/L), background solution (H_2O), sample 1 (MnO_2 and 1.5 mM/L oxalate), sample 2 (MnO_2 and 750 μM/L oxalate) by ion chromatograph. The results show that both two characteristic peaks were observed at the peak position of Mn^{2+}. The peak area is 3.098 μS min for the standard sample, 0.848 μS min for sample 1, and 0.375 μS min for sample 2, which corresponds to oxalate concentrations of the samples. Therefore, it is confirmed that MnO_2 nanosheets would be consumed in the existence of oxalate.

3.2. Optimization of experimental conditions

Before the MnO_2 nanosheets were used to detect oxalate, the amount of the nanosheets should be optimized. In the optimization experiments, the volume of added MnO_2 nanosheets varied from 1 μl to 7 μl. After adding MnO_2 nanosheets, the color of the TMB solution changed to blue due to the oxidation of TMB to oxTMB. As the volume of added MnO_2 nanosheets increases, the color of the solution is gradually dark (Fig. 3(A)). The results show that TMB can be oxidized without H_2O_2, which is in accordance with the former research (Liu et al., 2012). In the presence of HCl, the color of the solution turned yellow as shown in Fig. 3(B), indicating the termination of the reaction (Qiu et al., 2018). The termination of the reaction in low pH (< 1.0) can effectively enhance the absorbance of the oxidized TMB to 1.4 times under a very acid environment. (Bally and Gribnau, 1989). Subsequently, the absorbance spectrum of each well was detected after the termination. From Fig. 3(C), the characteristic absorption wavelength of the reaction can be confirmed at 460 nm for oxalate detection. The peak absorbance at 460 nm of those spectrums was analyzed (Fig. 3(D)). The peak absorbance exhibits a sharp rise to around 1.6 when the volume of MnO_2 nanosheets increases from 1 to 3 μl, and then the increase slows down with higher volume (4–7 μl). In order to ensure the high sensitivity and wide detection range in the measurement, 3 μl MnO_2 nanosheets was adopted for the further analysis.

Based on the previous optimization, the system of the MnO_2 nanosheets-TMB as a sensitive detector for oxalate determination was further optimized under different conditions. First, the interaction time between oxalate and MnO_2 nanosheets was investigated in the presence of 100 μM oxalate (Fig. 3 (E)). With the increase of the interaction time, the absorbance gradually declines, suggesting that more MnO_2 nanosheets were reduced by oxalate with longer time. After reacting for more than 10 min, only slight absorbance change can be observed. To shorten the detection time and obtain large absorbance changes, the interaction time was set as 10 min. Subsequently, the color reaction time between TMB and MnO_2 nanosheets was also investigated (Fig. 3(F)). 100 μl TMB was added into the MnO_2 nanosheets solution for reaction. The results show that no significant changes can be observed with different color reaction time. Therefore, an interaction time of 10 min and a color reaction time of 1 min were selected to implement the following colorimetric oxalate detection. pH in the samples should also be explored to ensure the best performance. It is reported that pH will affect the rate of reductive dissolution of MnO_2 in the presence of oxalate, and the highest reductive dissolution rate is at pH 1.6 ± 0.2 (Artamonova et al., 2013; Xyla et al., 1992). However, lower pH will affect TMB color development. So pH in oxalate solutions was adjusted to 3. Moreover, the effect of pH on the chromogenic reaction of MnO_2 nanosheets with TMB was also explored. The MnO_2 nanosheets and TMB were reacted in different pH environment (pH = 3, 4, 5) and then HCl was added to stop the reaction. As shown in the Fig. S1, different pH presents no significant change in color and the absorbances are almost unchanged, indicating that pHs would not affect the chromogenic reaction. Furthermore, since CO_2 was produced and H^+ was consumed in the reaction, the pH variation after the reaction of MnO_2 and oxalate (250 μM and 7.8 μM, pH = 3) was investigated compared to the sample without oxalate (Table S1). The results indicate that the pH after reaction has very slight change. Therefore it can be concluded that the consumption of H^+ and the production of CO_2 will not affect the pH of the solution during the reaction.

3.3. Analytical performance

Based on the optimized parameters, the analytical performance of the TMB-MnO_2 nanosheets system for oxalate detection was evaluated. Different concentrations of oxalate samples were prepared using gradient dilution from 4 mM to 9.8 μM. In order to calculate the limit of detection (LOD), the blank solution without oxalate was repeated in 10 wells. All the colorimetric experiments were analyzed by both the plate reader and the bionic E-eye system, and the analytical performance was also compared. As shown in Fig. 4(A) and (B), the response of the two instruments present S-shaped curves with good consistency. When the concentration of oxalate is lower than 7.8 μM or higher than 250 μM, the absorbance shows very slight changes. The TMB-MnO_2 nanosheets system demonstrates good linearity in the concentration range from 7.8 μM to 250 μM. The calibration plot of both the two instruments is shown in the inset, in which the bionic E-eye presents good linearity comparable to the commercial plate reader. Moreover, according to the 3σ rule, the LOD of the method using the two instruments was calculated and compared (Fig. 4(C)). The LOD using the plate reader is 0.83 μM, and that of the bionic E-eye is 0.91 μM. The reason of the slightly higher LOD of the bionic E-eye is that the bandwidth of the light source in bionic E-eye is wider than that of the plate reader, and the light source of the bionic E-eye will produce polychromatic light with less sensitivity. It is worth noting that the bionic E-eye presents comparable performance to the commercial plate reader with wide detection range and low LOD, and the bionic E-eye can be used to monitor the occurrence of initial urolithiasis in daily point-of-care applications considering the portability, low time cost and ease of use.

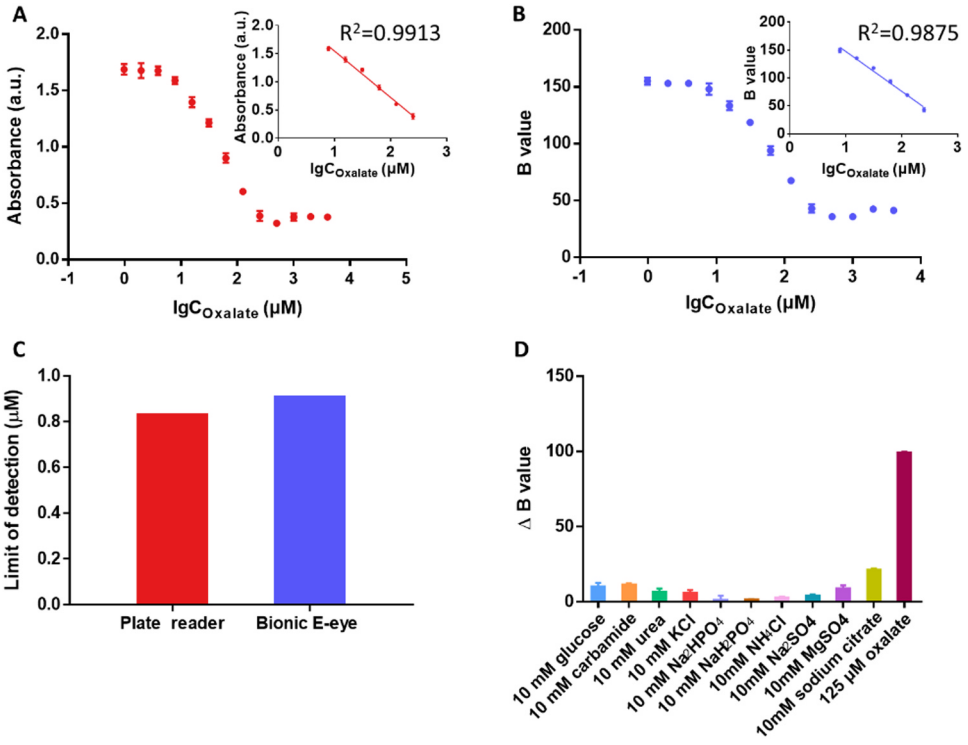

Fig. 4. The S-shaped response of the plate reader (A) and the bionic E-eye (B) in different concentrations of oxalate, and the insets show the linear detection ranges of the two instruments. (C)The comparison of LOD for the plate reader and bionic E-eye. (D) The selectivity study of the method for oxalate detection under different interfering chemicals.

Table 1
Results of oxalate determination for artificial urine samples.

Sample	Oxalate (μM)	Oxalate measured by bionic E-eye (μM)[a]	% Recovery of bionic E-eye	Oxalate measured by kit[a]	% Recovery of kit
1	100	92.20 ± 0.87	92.20	106.52 ± 2.61	106.52
2	50	46.38 ± 1.56	92.77	46.62 ± 4.00	93.24
3	25	24.24 ± 1.58	96.96	24.37 ± 1.64	97.48
4	10	10.40 ± 0.57	104.00	10.53 ± 0.76	105.30

[a] Mean value of three measurements ± standard deviation.

Further studies were performed to evaluate the potential interference of chemicals in human urine, including glucose, carbamide, urea, KCl, Na_2HPO_4, NaH_2PO_4, NH_4Cl, $MgSO_4$, Na_2SO_4, and sodium citrate (Fig. 4(D)). Compared to oxalate, these chemicals show very slight interference, even with a 80-fold concentration relative to oxalate, indicating the good selectivity of the TMB-MnO_2 nanosheets system.

3.4. Analysis of artificial urine samples

In order to evaluate the potential in-situ application of the proposed system for urinary oxalate detection, several artificial urine samples were analyzed based on standard curve method (Table 1) and standard addition method (Table S2). The real samples spiked with different oxalate concentrations were measured by the bionic E-eye system. The concentration of the measured oxalate is very close to that of the added oxalate. The recovery of the three spiked samples is higher than 92%, exhibiting the capability of the biosensor for oxalate quantification in human urine. And the results are also compared with kit for oxalate detection in which the two methods present very high consistency, validating the accuracy of our method for oxalate detection in urine samples.

Compared to other materials/methods for oxalate detection (Table 2), MnO_2 nanosheets-TMB methods demonstrates the lowest LOD and the shortest time cost. In plate reader, 96 wells are measured sequentially with a relatively long time cost. Our home-made bionic E-eye can photograph all 96 wells simultaneously, which significantly shortens the plate reading time and ensures that all wells are detected simultaneously. Furthermore, the bionic E-eye with small size features and high portability, which is more suitable for on-site detection and point of care application.

4. Conclusions

In this work, we developed a simple, rapid and sensitive colorimetric method using based on TMB-MnO_2 nanosheets for oxalate detection combining with a highly portable bionic E-eye system. Experimental conditions including the amount of MnO_2 nanosheets, interaction time of TMB-MnO_2, color reaction time, and pH have been optimized to ensure the ideal performance. The method shows a low LOD of 0.91 μM and a wide detection range from 7.8 μM to 250 μM with very good repeatability, long-term stability and high selectivity.

Table 2
The comparison of different materials/methods for oxalate detection.

Method/Material	LOD /μM	Average required time for one sample	Real sample	Portability	Ref.
TiO_2 nanoparticles/multiwalled carbon nanotubes modified electrode	33	> 30 min	Spinach	No	(Fakhari et al., 2012)
An electrode modified with Fe(III)-tris-(2-thiopyridone) borate	1000	> 12 h	N/A	No	(Rodríguez Ávila, 2012)
A carbon ionic liquid electrode modified with TiO_2-Fe nanoparticles	23	> 15 min	Urine	No	(Akhond et al., 2016)
Paper-based colorimetric device	10	30 min	Urine	Yes	(Worramongkona et al., 2018)
The plate reader	0.83	15 min	Urine	No	Our method
Bionic E-eye	0.91	11 min	Urine	Yes	Our method

Artificial urine samples were measured with good recovery to validate the performance for real sample analysis. Compared to other methods, the bionic E-eye based method shows the lowest LOD and the shortest time cost with high portability. We believe this approach will provide a promising platform for the clinical diagnosis of urolithiasis in the point-of-care applications.

CRediT authorship contribution statement

Ying Gan: Conceptualization, Validation, Data curation, Methodology, Writing - original draft, Writing - review & editing. **Ning Hu:** Conceptualization, Validation, Writing - original draft, Writing - review & editing. **Chuanjiang He:** Conceptualization. **Shuqi Zhou:** Data curation, Methodology. **Jiawei Tu:** Data curation, Methodology. **Tao Liang:** Data curation, Methodology. **Yuxiang Pan:** Investigation. **Dmitry Kirsanov:** Investigation, Resources. **Andrey Legin:** Investigation, Resources. **Hao Wan:** Conceptualization, Data curation, Methodology, Writing - original draft, Writing - review & editing. **Ping Wang:** Conceptualization, Data curation, Methodology, Writing - original draft, Writing - review & editing.

Acknowledgement

This study was supported by the RFBR-NSFC project #18-53-53016 GFEN_a, China (NSFC-RFBR Cooperation of China Grant No. 81811530116), National 973 Project of China (Grant No. 2015CB352101), Fundamental Research Funds for the Central Universities, China (Grant No. 2018QNA5018, 2018FZA5018) and Major Research and Development Project of Zhejiang Province, China (Grant No. 2019C03066).

Declaration of interests

None.

Appendix A. Supporting information

Supplementary data associated with this article can be found in the online version at doi:10.1016/j.bios.2019.01.026.

References

Akhond, M., Absalan, G., Tafakori, A., Ershadifar, H., 2016. Simultaneous determination of thiocyanate and oxalate in urine using a carbon ionic liquid electrode modified with TiO2-Fe nanoparticles. Anal. Bioanal. Chem. Res. 3 (1), 73–86.
Akoudad, S., Szklo, M., McAdams, M.A., Fulop, T., Anderson, C.A., Coresh, J., Kottgen, A., 2010. Correlates of kidney stone disease differ by race in a multi-ethnic middle-aged population: the ARIC study. Prev. Med. 51 (5), 416–420.
Artamonova, I., Gorichev, I., Godunov, E., 2013. Kinetics of manganese oxides dissolution in sulphuric acid solutions containing oxalic acid. Engineering 5 (09), 714.
Bally, R.W., Gribnau, T.C.J., 1989. Some aspects of the chromogen 3,3',5,5'-Tetramethylbenzidine as hydrogen donor in a horseradish-peroxidase assay. J. Clin. Chem. Clin. Biol. 27 (10), 791–796.
Boyce, C.J., Pickhardt, P.J., Lawrence, E.M., Kim, D.H., Bruce, R.J., 2010. Prevalence of urolithiasis in asymptomatic adults: objective determination using low dose non-contrast computerized tomography. J. Urol. 183 (3), 1017–1021.
Chutipongtanate, S., Thongboonkerd, V., 2010. Systematic comparisons of artificial urine formulas for in vitro cellular study. Anal. Biochem. 402 (1), 110–112.
Coe, F.L., Worcester, E.M., Evan, A.P., 2016. Idiopathic hypercalciuria and formation of calcium renal stones. Nat. Rev. Nephrol. 12 (9), 519–533.
Dey, N., Kumari,, N., Bhagat, D., Bhattacharya, S., 2018. Smart optical probe for 'equipment-free' detection of oxalate in biological fluids and plant-derived food items. Tetrahedron.
Fakhari, A.R., Rafiee, B., Ahmar, H., Bagheri, A., 2012. Electrocatalytic determination of oxalic acid by TiO 2 nanoparticles/multiwalled carbon nanotubes modified electrode. Anal. Methods-UK 4 (10), 3314–3319.
Guan, G., Zhang, S., Liu, S., Cai, Y., Low, M., Teng, C.P., Phang, I.Y., Cheng, Y., Duei, K.L., Srinivasan, B.M., Zheng, Y., Zhang, Y.W., Han, M.Y., 2015. Protein induces layer-by-layer exfoliation of transition metal dichalcogenides. J. Am. Chem. Soc. 137 (19), 6152–6155.
He, Y., Wang, Z.R., Long, D.Y., 2016. Direct visual detection of MnO2 nanosheets within seconds. Anal. Bioanal. Chem. 408 (4), 1231–1236.
Inoue, K., Aikawa, S., Fukushima, Y., 2018. Colorimetric detection of oxalate in aqueous solution by a pyrogallol red-based Cu(2+) complex. Lumin.: J. Biol. Chem. Lumin. 33 (2), 277–281.
Kai, K., Yoshida, Y., Kageyama, H., Saito, G., Ishigaki, T., Furukawa, Y., Kawamata, J., 2008. Room-temperature synthesis of manganese oxide monosheets. J. Am. Chem. Soc. 130 (47), 15938–15943.
Li, H., Chai, X.S., DeMartini, N., Zhan, H., Fu, S., 2008. Determination of oxalate in black liquor by headspace gas chromatography. J. Chromatogr. A 1192 (2), 208–211.
Lin, L., Shi, D.M., Li, Q.F., Wang, G.F., Zhang, X.J., 2016. Detection of T4 polynucleotide kinase based on a MnO2 nanosheet-3,3 ',5,5 '-tetramethylbenzidine (TMB) colorimetric system. Anal. Methods-UK 8 (20), 4119–4126.
Liu, J., Meng, L.J., Fei, Z.F., Dyson, P.J., Jing, X.N., Liu, X., 2017. MnO2 nanosheets as an artificial enzyme to mimic oxidase for rapid and sensitive detection of glutathione. Biosens. Bioelectron. 90, 69–74.
Liu, X., Wang, Q., Zhao, H.H., Zhang, L.C., Su, Y.Y., Lv, Y., 2012. BSA-templated MnO2 nanoparticles as both peroxidase and oxidase mimics. Analyst 137 (19), 4552–4558.
Liu, Z., Ma, R., Ebina, Y., Takada, K., Sasaki, T., 2007. Synthesis and delamination of layered manganese oxide nanobelts. Chem. Mater. 19 (26), 6504–6512.
Maya, F., Estela, J.M., Cerda, V., 2011. Multisyringe ion chromatography with chemiluminescence detection for the determination of oxalate in beer and urine samples. Microchim. Acta 173 (1–2), 33–41.
Mitra, P., Pal, D.K., Das, M., 2018. Does quality of drinking water matter in kidney stone disease: a study in West Bengal, India. Investig. Clin. Urol. 59 (3), 158–165.
Munoz, J.A., Lopez-Mesas, M., Valiente, M., 2010. Development and validation of a simple determination of urine metabolites (oxalate, citrate, uric acid and creatinine) by capillary zone electrophoresis. Talanta 81 (1–2), 392–397.
Parmar, M.S., 2004. Kidney stones. BMJ 328 (7453), 1420–1424.
Perello, J., Sanchis, P., Grases, F., 2005. Determination of uric acid in urine, saliva and calcium oxalate renal calculi by high-performance liquid chromatography/mass spectrometry. J. Chromatogr. B 824 (1–2), 175–180.
Pundir, C.S., Chauhan, N., Rajneesh, Verma, M., Ravi, 2011. A novel amperometric biosensor for oxalate determination using multi-walled carbon nanotube-gold nanoparticle composite. Sens. Actuators B-Chem. 155 (2), 796–803.
Pundir, C.S., Kuchhal, N.K., Thakur, M., Satyapal, 1998. Determination of plasma oxalate with chloride ion insensitive oxalate oxidase. Indian J. Biochem. Biophys. 35 (2), 120–122.
Pundir, C.S., Satyapal, 1998. Determination of urinary oxalate with CI- and NO3- insensitive oxalate oxidase purified from sorghum leaf. Clin. Chem. 44 (6 Pt 1), 1364–1365.
Qiu, X.X., Zhong, L.J., Gan, Y., Su, K.Q., Hu, S.H., Wang, P., 2018. A method combining a kit with the bionic e-eye for rapid on site detection of diarrhetic shellfish poisoning. Anal. Methods-Uk 10 (22), 2604–2613.
Rodríguez Ávila, J.A., 2012. Amperometric biosensor for oxalate determination in urine using sequential injection analysis.
Romero, V., Akpinar, H., Assimos, D.G., 2010. Kidney stones: a global picture of prevalence, incidence, and associated risk factors. Rev. Urol. 12 (2–3), e86–96.
Somani, B.K., Aboumarzouk, O., Traxer, O., Baard, J., Kamphuis, G., de la Rosette, J., 2016. Medical expulsive therapy for ureteral stones: where do we go from here? Nat. Rev. Urol. 13 (10), 608–612.
Stamatelou, K.K., Francis, M.E., Jones, C.A., Nyberg, L.M., Curhan, G.C., 2003. Time trends in reported prevalence of kidney stones in the United States: 1976–1994.

Kidney Int. 63 (5), 1817–1823.
Su, K.Q., Zou, Q.C., Zhou, J., Zou, L., Li, H.B., Wang, T.X., Hu, N., Wang, P., 2015. High-sensitive and high-efficient biochemical analysis method using a bionic electronic eye in combination with a smartphone-based colorimetric reader system. Sens. Actuators B-Chem. 216, 134–140.
Turney, B.W., Reynard, J.M., Noble, J.G., Keoghane, S.R., 2012. Trends in urological stone disease. BJU Int. 109 (7), 1082–1087.
Wan, Y., Qi, P., Zhang, D., Wu, J., Wang, Y., 2012. Manganese oxide nanowire-mediated enzyme-linked immunosorbent assay. Biosens. Bioelectron. 33 (1), 69–74.
Worramongkona, P., Seeda, K., Phansomboon, P., Ratnarathorn, N., Chailapakul, O., Dungchai, W., 2018. A simple paper-based colorimetric device for rapid and sensitive urinary oxalate determinations. Anal. Sci. : Int. J. Jpn. Soc. Anal. Chem. 34 (1), 103–108.
Xyla, A.G., Sulzberger, B., Luther, G.W., Hering, J.G., Vancappellen, P., Stumm, W., 1992. Reductive dissolution of manganese(III,IV) (hydr)oxides by oxalate – the effect of pH and light. Langmuir 8 (1), 95–103.
Yu, H.L., Zheng, L., 2016. Manganese dioxide nanosheets as an optical probe for photometric determination of free chlorine. Microchim Acta 183 (7), 2229–2234.
Yuan, J., Cen, Y., Kong, X.J., Wu, S., Liu, C.L.W., Yu, R.Q., Chu, X., 2015. MnO2-nanosheet-modified upconversion nanosystem for sensitive turn-on fluorescence detection of H2O2 and glucose in blood. ACS Appl. Mater. Interfaces 7 (19), 10548–10555.
Zhai, Q.Z., Zhang, X.X., Liu, Q.Z., 2006. Catalytic kinetic spectrophotometry for the determination of trace amount of oxalic acid in biological samples with oxalic acid-rhodamine B-potassium dichromate system. Spectrochim. Acta A 65 (1), 1–4.
Zhai, W.Y., Wang, C.X., Yu, P., Wang, Y.X., Mao, L.Q., 2014. Single-layer MnO2 nanosheets suppressed fluorescence of 7-hydroxycoumarin: mechanistic study and application for sensitive sensing of ascorbic acid in vivo. Anal. Chem. 86 (24), 12206–12213.
Zhang, S.R., Wang, Q., Tian, G.H., Ge, H.G., 2014. A fluorescent turn-off/on method for detection of Cu2+ and oxalate using carbon dots as fluorescent probes in aqueous solution. Mater. Lett. 115, 233–236.
Zuo, G.K., Jiang, X.J., Liu, H., Zhang, J.Y., 2010. A novel urinary oxalate determination method via a catalase model compound with oxalate oxidase. Anal. Methods-UK 2 (3), 254–258.